Investigation of the climatology of low-level jets over North America in a convection-permitting WRF simulation

删除了： high-resolution

Xiao Ma[1,2], Yanping Li[1,2], Zhenhua Li[1], Fei Huo[1]

[1]Global Institute for Water Security, University of Saskatchewan, 11 Innovation Blvd, Saskatoon, SK, S7N 3H5, Canada

[2]School of Environment and Sustainability, University of Saskatchewan, 117 Science Place, Saskatoon, SK, S7N 5C8, Canada

Correspondence to: Yanping Li (yanping.li@usask.ca)

Abstract. In this study, we utilized a high-resolution (4 km) convection-permitting Weather Research Forecasting (WRF) simulation spanning a 13-year period (2000-2013) to investigate the climatological features of Low-level Jets (LLJs) over North America. The 4-km simulation enabled us to represent the effects of orography and the underlying surface on the boundary layer winds better. Focusing on the continental US and the adjacent border regions of Canada and Mexico, this study characterizes the spatial distribution, seasonal patterns, and diurnal fluctuations of northerly/southerly LLJ occurrence frequencies. This paper not only identified several well-known large-scale LLJs in North America, such as the southerly Great Plains LLJ and the summer northerly California coastal LLJ, but also the Quebec northerly LLJ, which gets less focus before. Moreover, the high-resolution simulation revealed climatic characteristics of weaker and smaller-scale LLJs or low-level wind maxima in regions with complex terrains, such as the northerly LLJs in the foothill regions of the Rocky Mountains and the Appalachian during the winter. Additionally, the different thermal and dynamic mechanisms forming significant LLJs near the Great Plains, California, and Quebec are investigated. This study provides valuable insights into the climatological features of LLJs in North America and the high-resolution simulation offers a more detailed understanding of LLJ behavior near complex terrains and other smaller-scale features.

1. Introduction

A low-level jet (LLJ) is described as the fast-moving air ribbon located in the lower atmosphere most of the time (Bonner, 1968; Rife et al., 2010). Many of the world's LLJs have been studied, such as the Great Plains LLJ over the central US (Bonner, 1968; Zhong et al., 1996), the Somali LLJ over eastern Africa (Munday et al., 2021), and the South American LLJ over the east Andes Mountains (Montini et al., 2019). Other studies extend beyond in-land LLJs to encompass offshore coastal LLJs such as the California LLJs (Parish, 2000) and North African Coastal LLJ (Soares et al., 2018). A kind of mesoscale weather system, an LLJ has a relatively small vertical range of usually only a few hundred meters, but its width can reach several hundred kilometers. LLJs are closely related to precipitation and even extreme events, and they can transfer abundant water vapor to the downwind regions, providing favorable dynamic conditions for rainfall (Walters and Winkler, 2001; Hodges and Pu, 2019). Meanwhile, researchers have long been interested in investigating their features, because LLJs also affect various processes such as wind power development, air pollution transportation, and urban heat islands; the wind turbines would be influenced by positive wind shear and downward entrainment from the LLJs above them, assisting in extracting energy from the strong wind belt inside LLJs (Gadde and Stevens 2021; Ma et al., 2022). LLJ-related horizontal transportation is beneficial to pollutant removal (Sullivan et al. 2017). The LLJs can enhance the turbulent mixing in the boundary layer thereby decreasing the atmospheric stability, helping pollution diffusion, and weakening urban heat island intensity (Hu et al., 2013).

Since the mid-20th century, scientists have used regular rawinsonde observations to investigate the characteristics of LLJs. Applying rawinsondes to investigate the Great Plains LLJ in the central US, Bonner (1968), Mitchelle et al. (1995), and Walters et al. (2008) studied its distribution, seasonal activity, horizontal and vertical structure, and diurnal features and established the climatology of the Great Plains LLJ during warm seasons. As well as rawinsondes, radar systems and wind profilers are useful tools for characterizing LLJs. Frisch et al. (1992) observed a typical LLJ process using Doppler weather radar in North Dakota and identified that the friction on the surface of the boundary layer is important in the early stages of LLJ development. Using long-term wind profiler measurement, Miao et al. (2018) interpreted the climatology of LLJs in Beijing and Guangzhou, concluding that the frequency values of LLJs in these two cities are 13.0% and 4.9%, respectively. Moreover, Smith et al. (2019) used the Plains Elevated Convection at Night (PECAN) observations to conduct high-quality measurements of nocturnal LLJs with wide spatial and temporal resolutions. They found that sudden changes in LLJ structure typically result from the spatial evolution of the LLJ.

删除了： generally

删除了： Because

删除了： (Hu et al., 2013; Sullivan et al. 2017;

删除了： , Ma et al., 2022), researchers have long been interested in investigating their features.

However, there are some disadvantages of observational research that should be noted. First, regular rawinsonde data only contain measurements at two daily time points (00 UTC and 12 UTC), which cannot fully capture LLJs' diurnal variations. The time density of observations is therefore coarse, and coastal areas lack regular high-density measurements, making the study of coastal LLJs challenging (Mitchell et al., 1995). Second, heterogeneities in the rawinsonde records, such as variations in station locations, radiosonde types, and archiving procedures, may also complicate the use of these observations in climate research. Third, rawinsonde measurements taken at a single point are not able to capture horizontal shear and environmental conditions (Chen et al., 2005). Although observations platforms such as radar or field projects like PECAN can compensate to some extent for this lack of observational data, these approaches are still limited by the spatial coverage of their measurement platforms (Smith et al., 2019).

Because of these problems with observational methods, researchers have chosen reanalysis datasets as an alternative for investigating LLJs. Reanalysis data have relatively better spatial and temporal coverage than rawinsonde measurements, incorporate observations into the preliminary model simulations, provide more comprehensive variables through assimilation, and contain broader domains. Rife et al. (2010) highlighted the global distribution of identified nocturnal LLJs using reanalysis data with a horizontal grid spacing of 40 km, and even successfully extracted some previously unknown jets, like Tarim nocturnal LLJ in northwest China, Ethiopia nocturnal LLJ, and Namibia–Angola nocturnal LLJ. Doubler et al. (2015) applied the North American Regional Reanalysis (NARR) dataset (~32 km) to generate long-term LLJ climatology in North America. Consistent with previous records, Doubler's results supplemented the description of some smaller-scale LLJs. Similarly, Montini et al. (2019) compared and validated the performance of five different reanalysis datasets in identifying LLJs. Their results showed the 38-year climatology of South American LLJs with ERA-Interim data (~79 km).

Scientists have also conducted studies based on numerical simulations, which can more accurately represent LLJs than reanalysis data sets, especially in the vertical direction, thereby yielding new insights into LLJs' features. Tang et al. (2017) used an ensemble of dynamically downscaling regional climate simulations to generate the climatology of Great Plains LLJ and predicted that the LLJ will occur more frequently during the nighttime in spring and summer in mid-21st century. Jiménez-Sánchez et al. (2019) conducted a simulation for LLJs over the Orinoco River Basin by dynamic downscaling of the Weather Research and Forecasting model (WRF). The simulation represented the jet streaks better than previous studies within a broader region of wind enhancement and illustrated more detailed diurnal

设置了格式：英语(美国)

删除了： perform more extensive measurements

删除了： .

evolution. Nevertheless, most general numerical simulations still represent the convective processes by the parameterization scheme, which generates uncertainty in the results. These issues can be addressed by using convection-permitting models with grid spacing under 5 km that adequately simulate the convections and other small-scale processes (Liu et al., 2017, Li et al., 2019, Kurkute et al., 2020). Convection-permitting modeling describes the underlying surface more accurately than coarse-resolution simulations and reanalysis data and shows ability in investigations of LLJs near complex mountain areas. Du and Chen (2019) analyzed the LLJs over southern China by using 4-km WRF model and revealed a solid relationship between the mesoscale lifting of LLJs and the convection's initiation. They also highlighted the importance of coastal terrain. Overall, the finer-resolution tools tend to show more comprehensive and precise results, offering detailed and accurate references to LLJs.

The formation mechanisms of LLJs have been studied extensively by researchers. In explaining the diurnal cycle feature of the Great Plains LLJ, the inertial oscillation theory proposed by Blackadar (1957) and Stensrud (1996) suggests that the LLJ is related to the friction change in the boundary layer. During the night, the jet-core wind is enhanced after decoupling with near-surface friction. Holton (1967) and Parish (2000) developed the thermal wind adjustment theory, which suggests that the horizontal pressure gradient changes because the atmosphere over sloping terrain is warmer or because sea-land contrast influences the diurnal cycle of wind. Additionally, LLJs can also be formed due to synoptic system forcing, as proposed by Uccellini et al. (1987) and Saulo et al. (2007). However, convection-permitting models can help explain how LLJs form because they have precise descriptions of weather systems and underlying orography. Using 4-km simulations, Fu et al. (2018) and Zhang et al. (2019) analyzed the evolution of LLJs over mountainous areas in eastern and southwestern China, respectively. They concluded that inertial oscillation plays a prominent role in and is responsible for the local precipitation peak at a certain time. Besides, Shapiro et al. (2016) argued that the formation of some LLJs may not be impacted by a single factor and that a unified theory analysis is thus required. Thus, a dataset that offers more information must be very popular. All these studies have shown that convection-permitting models, with both finer coverage and resolutions, are a powerful tool for LLJ climatology research.

In this study, we utilize the 4-km convection-permitting WRF simulation (Liu et al., 2017) to compile a comprehensive LLJ climatology across North America and investigate the features of major LLJ systems in the region with improved spatial and temporal resolutions. Section 2 introduces the model configuration and the criteria for LLJ identification,

删除了： promise

删除了： In

删除了：), it is suggested

删除了： diurnal cycle feature of the Great Plains LLJ

删除了： The purpose of

删除了： is to use

删除了： model

删除了： produce

删除了： detailed

删除了： . This paper focuses on

删除了： LLJs in

删除了： areas of North America and aims to provide alternative dataset sources

删除了： the finer

删除了： resolution for the LLJs in this region and provide more helpful tools for LLJs-related studies in other disciplinary…

Section 3 presents the characteristics of LLJ frequencies in North America, and Section 4 illustrates the analysis of the background and mechanisms in several LLJ cases. Finally, Section 5 provides the discussion and conclusion.

2. Model configuration and methods

2.1 WRF setup

This study utilized a convection-permitting Weather Research and Forecasting (WRF) dataset (Liu et al. 2017, Data available at: https://rda.ucar.edu/datasets/ds612.0/) with a horizontal resolution of 4 km over North America, without nesting. The domain covers the entire continental US, Southern Canada, and Northern Mexico, as illustrated in Figure 1. The simulation provides three-dimensional data at a temporal resolution of 3 hours, resulting in 8-time steps per day. In the vertical direction, the data have 51 eta levels and can reach 50 hPa. And it should be noted that there are five layers under 500-m height and nine layers under 1 km are outputted above ground level, which means the WRF has the better ability than other coarse modelling, to capture the LLJs occurring in the boundary layer. Considering the computational cost for high-resolution modelling, this simulation period spans from 1st October 2000 to 30th September 2013, and the six-hourly ERA-Interim reanalysis dataset of 0.7° resolution was used as input for the climate simulation, the vertical layer depth of the forcing ERA-Interim data under 5 km is about 0.3-1.4 km (Hoffmann & Spang, 2022). The simulation did not apply any cumulus parameterization scheme due to the fine horizontal grid spacing, but other sub-grid scale processes were parameterized by various physical schemes: the rapid radiative transfer model (RRTMG) (Iacono et al., 2008) was used for simulating longwave and shortwave radiations, the Yonsei University (YSU) scheme was used for representing the planetary boundary layer (Hong et al., 2006), and the Noah-MP model was used for computing surface processes (Niu et al., 2011). In this study, the planetary boundary layer scheme is retained. Nonetheless, it should be noted that this would introduce uncertainties to the simulation in the vertical direction, especially in regions with complex topography.

删除了：.

删除了：good

删除了：The

删除了：.

删除了：, but

设置了格式

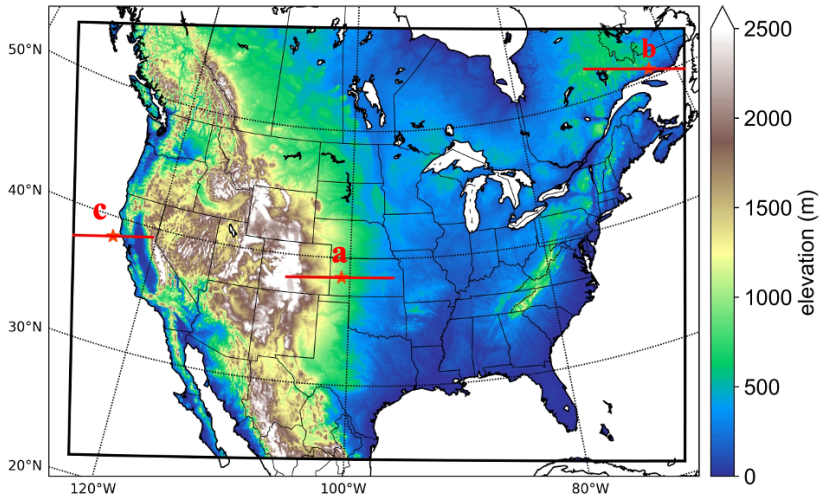

Figure 1. Study domain of this convection-permitting model. The colors represent the elevation. The red lines and stars show the positions of investigated cross-section and jets in Section 4.

2.2 Methodology

Using the threshold criteria proposed by Bonner (1968), this study identifies LLJs from the vertical wind profile of each grid point in the model output data. LLJs are present when the following conditions are met: (1) the height of the LLJ core maximum wind speed is below 3 km above the ground level (AGL); (2) the maximum wind speed is greater than or equal to 12 m s-1; (3) from the height of the wind maxima to the height of the next minimum value or 3-km height (whichever is lower), the velocity of winds drop by at least 6 m s-1; (4) the wind speed drops by at least 6 m s-1 below the level of wind maxima. Considering the importance of the meridional LLJ for heat and water vapor transport, this study addresses their frequencies in different meridional directions. According to Walter et al. (2008) and Doubler et al. (2015), the criteria for identifying different meridional LLJs are as follows: for southerly LLJs (S-LLJs), the jet-core wind direction is between 113° and 247°; for northerly LLJs (N-LLJs), the jet-core direction is between 293° and 67°. These criteria are used in this study.

Based on the identification criteria above, we determined if the LLJ existed at each grid point and consequently counted the occurrences of S-LLJs and N-LLJs. We also calculated the frequencies of LLJs in different seasons or

time steps. The frequency is defined as the percentage of the total number of occurrences for the selected accumulation period. We generated the frequency distribution maps for LLJs climatology in North America, which are illustrated in Section 3.

3. The climatology of North American LLJs

3.1 Analysis of atmospheric circulation

This study adopts model data to capture the climatological features of LLJs in North America. Considering the relationship between LLJs and synoptical systems, we evaluated the ability of the convection-permitting model to simulate the background atmospheric circulation. Figure 2 depicts the simulated climatology of geopotential heights at 500 hPa and sea-level pressure isobars for summer and winter. In summer, at a height of 500 hPa (Figure 2a), In summer, the model depicts a trough in the east of the continental US, a ridge over the Rocky Mountains, and the upper-air subtropical anticyclone crossing the southern US. At sea level (Figure 2b), the model captures the Azores High-Pressure area in the Atlantic Ocean and the Hawaiian High-Pressure area in the Pacific.

In winter, the contours at the pressure value of 500 hPa (Figure 2c) show stronger fluctuating characteristics: the eastern trough and western ridge over the continent strengthen, and the polar vortex extends to the northern US, while most of North America is controlled by a cold high-pressure system. In addition, the subtropical anticyclone is too weak to be found within the study domain. On the other hand, most of North America is controlled by a cold high-pressure system at sea level (Figure 2d), and parts of the Icelandic Low and Aleutian Low appear on both east and west of Canada, even though their centers are not captured in the domain. To summarize, the convection-permitting model can simulate the features of semi-permanent centers of atmospheric circulations in North America, thus demonstrating its strength in identifying the LLJs in this area.

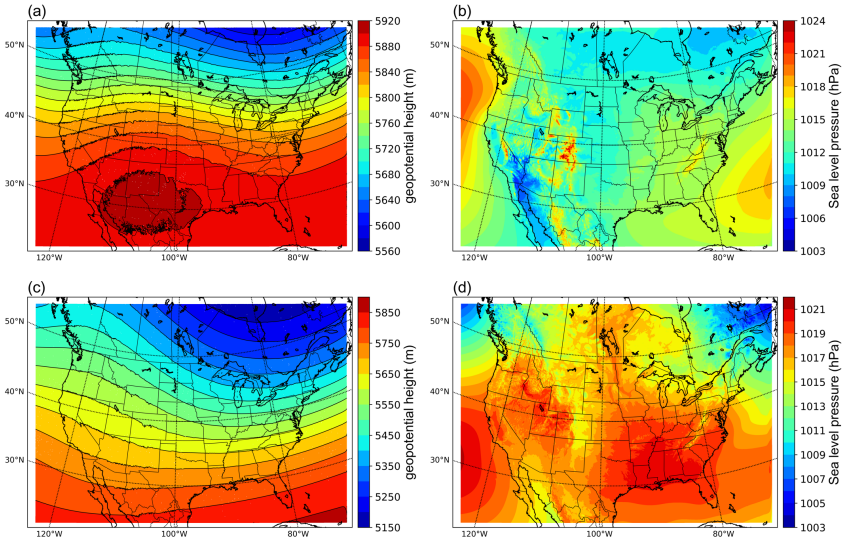

Figure 2. Climatology of atmospheric circulations simulated by the convection-permitting model: (a) summer 500 hPa geopotential height; (b) sea-level pressure in summer; (c)-(d) the same variables but in winter.

3.2 Seasonal variations of LLJs

3.2.1 Northerly LLJs

Figure 3 shows the frequency distribution of N-LLJ in four seasons, in which the frequency represents the ratio between the seasonal total number of LLJs occurrence and the total time steps in each season. Clearly, the California coastal LLJ is strongest in summer (June, July, and August (JJA)), with a large area of N-LLJ frequency greater than 25%, extending from the southern Oregon coast to the central California coast. Regions with a frequency greater than 5% can even extend to the Pacific Ocean near northern Baja California. However, from summer to autumn (September, October, and November (SON)), the frequency of this LLJ decreases sharply, with a frequency of only 5%-15% in the core region, and it is only distributed on the northern coast of California. In winter (Dec, Jan, and Feb (DJF)) it occurs very infrequently (~3%).

On the other hand, various N-LLJ phenomena occur frequently in the cold season. These N-LLJs are mainly located near the eastern slopes of special terrains such as the Rocky Mountains, Appalachian Mountains, and the Quebec

Labrador Plateau. In winter, high frequencies (>10%) are observed from western Alberta to Oklahoma, within which hot spots are distributed sporadically in Alberta, Montana, Wyoming, and Colorado. These hot spots have frequencies of about 20%, especially in the region between Colorado and Wyoming. In over 25% of the wind profiles, the N-LLJs can even be extracted. The N-LLJs over the Eastern US coast mainly extend from Maine to South Carolina, and their highest frequency can reach about 15%-20%. The N-LLJs in eastern Quebec also occur most frequently in winter (>25%). Over Hudson Bay, the simulation can also detect the N-LLJ from about 10% of the time steps. The frequencies of all the N-LLJs mentioned above decline significantly in spring, and it is hard to detect them in summer as the frequencies are mostly less than 5%.

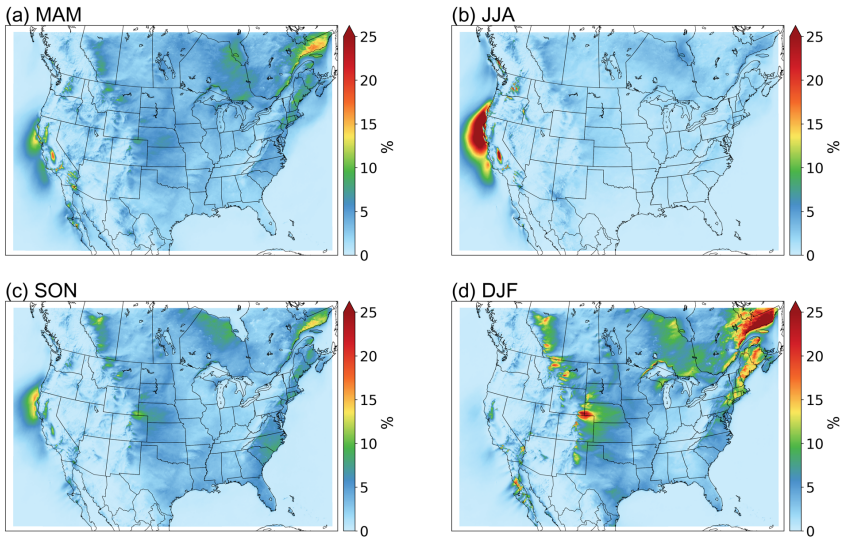

Figure 3. Seasonal occurrence frequency of N-LLJs. Frequency shown here is calculated by counting the number of occurrences of LLJs in each three-hourly time step and then dividing the total number of LLJs in each season by the number of time steps in that season.

3.2.2 Southerly LLJs

As to the climatology of S-LLJs in different seasons (see Figure 4), in winter, in the broad region extending from the south Texas-west Gulf of Mexico to southern Iowa, the frequencies of S-LLJs exceed 10%. The greatest frequencies of S-LLJs (>20%) are found along the border between northeastern Mexico and the United States. In addition, about

15% of the simulated wind profiles in south-central Texas are identified as S-LLJs. In the spring (March, April, and May), the frequency expands significantly in >10% of areas, with clear S-LLJ distributions detected in Manitoba, Saskatchewan, and other parts of Canada. The highest frequencies are still found in the Texas-Mexico area, where the magnitude of these frequencies increases to over 25%. This region also extends northward to occupy most of Texas. In winter, S-LLJs with occurrence frequencies of above 15% extend to near Colorado and Nebraska.

In summer, the area with frequencies greater than 10% no longer extends to the central Canadian prairie provinces and Tennessee. The S-LLJs over the western Gulf of Mexico are also difficult to identify with modeled data, and their frequency is close to 0%. In contrast, the area with frequencies exceeding 25% extends northward in summer and is roughly divided into three parts distributed respectively in the northeast Mexico-Texas border, west-central Texas, and the central US Great Plains (western Oklahoma and southern Kansas). The regions where more than 15% of the wind profiles are identified as S-LLJ also expand from Colorado to near South Dakota.

In the fall, the magnitude of the frequency of S-LLJs decreases dramatically in the central US Plains and Texas. The frequency still maintains a level greater than 15% in most areas, but with a maximum frequency of only 20% and sporadically located in southwest Texas. The frequencies greater than 10% again expand northward and eastward in this season, reaching Manitoba and Ontario.

There are also several S-LLJs on a smaller scale that can be seen on the seasonal S-LLJ climatology map. In spring, a narrow region of S-LLJs with a frequency greater than 5% on the eastern side of the Appalachians extends from Georgia through the western Atlantic to southern Nova Scotia. Over the Atlantic near eastern Maryland, the frequency of the S-LLJ can exceed 10%. In summer, this narrow frequency belt still exists and has the same coverage, but the magnitude of the frequency decreases and the frequency >10% is no longer visible. In winter, a region where S-LLJ frequency is >5% extends from southwest Oregon to the west coast of British Columbia of Canada. But in spring, S-LLJs with frequencies >5% occur only over the ocean west of British Columbia. As for the summer, S-LLJs are almost undetectable in this region.

删除了： vf

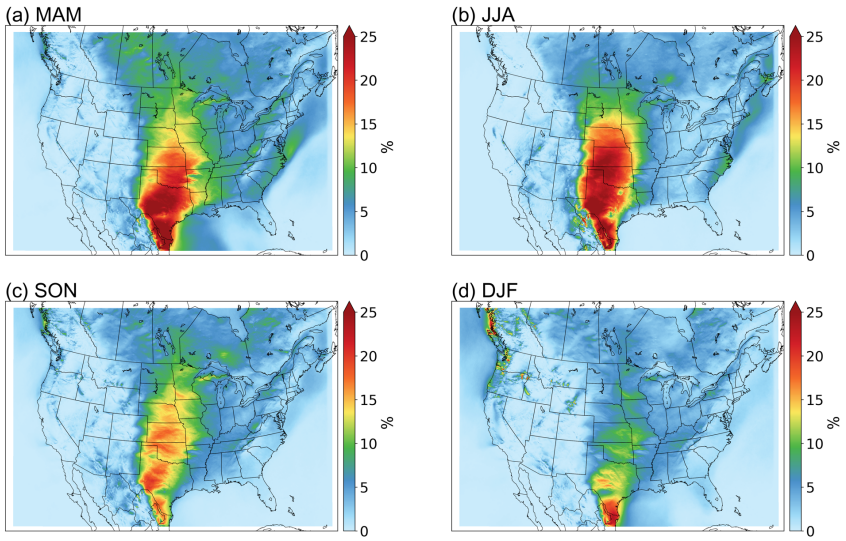

Figure 4. Seasonal frequency of S-LLJs.

To summarize, for the LLJ systems that have been investigated by many researchers, the convection-permitting WRF model performs well in observing the Great Plains S-LLJ and California coastal N-LLJ during the summer. But as to the winter LLJs that lack attention, it is essential to compare and validate the occurrence and features revealed by WRF simulation. Therefore, the ERA5 reanalysis dataset is applied in this study for capturing the LLJs in winter using the same criterion. Appendix after the text shows the results of the comparison between ERA5 and WRF simulation.

3.3 Diurnal variations of LLJs

To show the diurnal features of the LLJs, we selected summer and winter as the representative seasons because S-LLJs and N-LLJs occur most frequently in these seasons, respectively. Below, the descriptions are divided into N-LLJs and S-LLJs.

删除了：.

3.3.1 Northerly LLJs

The California coastal N-LLJ is the most highlighted low-level jet system in this region in summer. As seen in Figure 5, it occurs throughout the day over the eastern Pacific Ocean from Oregon to the California coast. Figure 5 also shows that the California Coastal N-LLJ has diurnal characteristics: from 21 UTC (1 pm LST in California), the low-level

删除了：,

jet begins to develop, with a N-LLJ frequency of >30%, expanding until it reaches its maximum at 03 UTC – 06 UTC. Then the high-frequency coverage of the California coastal LLJ gradually shrinks, reaching the minimum at 18 UTC and only existing off the northwest coast of California.

删除了： At the same time, the N-LLJ over the Hudson Bay Plain is also at its maximum frequency (>5%) from 03 UTC – 06 UTC, but it rarely occurs at other time steps.

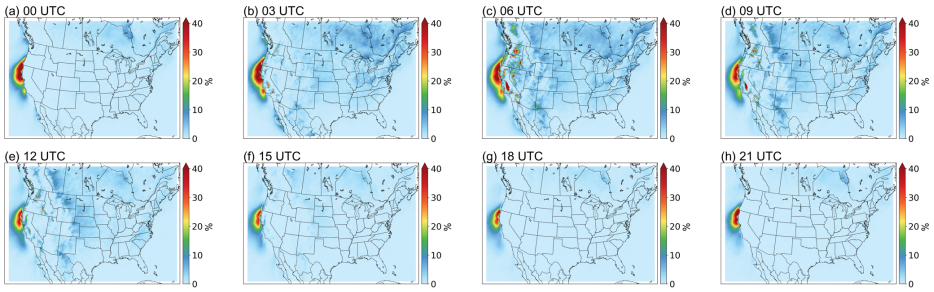

Figure 5. Diurnal frequency of N-LLJs in the summer (JJA).

In winter (Figure 6), three types of N-LLJs over the Hudson Bay Lowlands, the eastern slopes of the Quebec Labrador Plateau, and the Appalachians display similar diurnal fluctuations. All three N-LLJs reach their highest frequency at 03 UTC (10 pm EST) and their lowest at 18 UTC (1 pm EST). The only difference among the three types is that the smallest frequency of the Quebec N-LLJ still endures at a level of greater than 15%, while the other two N-LLJs mostly have frequencies of about 5%. The smallest frequency (~5%) of N-LLJs occurs downstream of the Rocky Mountains (over Alberta, Montana, and Kansas) at 21 UTC. In the subsequent development stage, the changes in the sporadic hot spots distributed near the eastern boundary of the Rocky Mountains are more significant. As seen in Figure 6, frequency starts growing from 00 UTC and then peaks at 12 UTC, especially the wind maxima located in Colorado, Wyoming, and Kansas, where the highest frequency can be >25%.

删除了： Plain

删除了： .

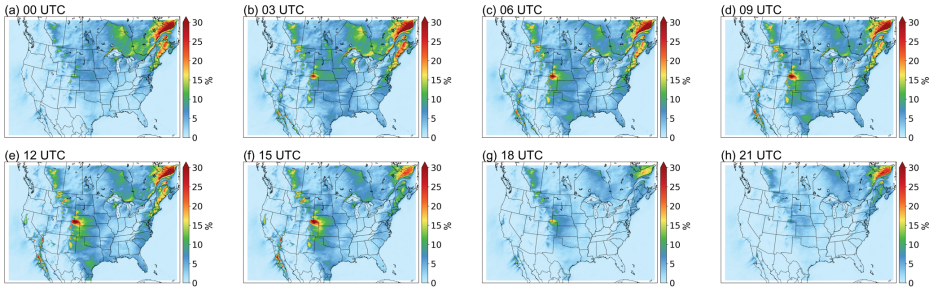

Figure 6. Diurnal frequency of N-LLJs in winter (DJF).

3.3.2 Southerly LLJs

In summer, the Great Plains S-LLJ occurs more frequently than in other seasons, and its diurnal variability is also the strongest in this season (see Figure 7). At noon local time and in the afternoon (18 UTC – 00 UTC), almost no S-LLJs occur over the central US (frequency <5% or about 0%). In contrast, the Great Plains LLJ begins to develop at 03 UTC, when a frequency of over 25% extends from Mexico to Kansas. It reaches maximum strength at midnight (06 UTC – 09 UTC), when the frequency reaches over 30% and the high-frequency coverage enlarges to the Dakotas, the border of the eastern Rocky Mountains, and western Minnesota, Missouri, and Louisiana. Summer S-LLJs are also active in southern Canada at night and in the early morning. In Saskatchewan, Manitoba, and central Ontario (03 UTC – 12 UTC, as shown in Figure 7), S-LLJs are found with frequency >15%. In the eastern US and Atlantic, S-LLJs occur most frequently at midnight (03 UTC – 06 UTC).

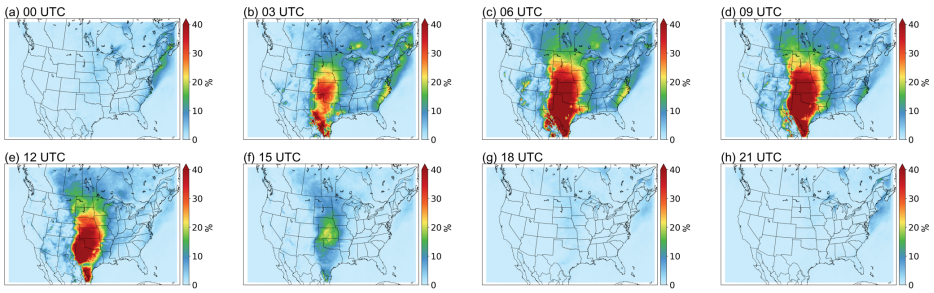

Figure 7. Diurnal frequency of S-LLJs in summer (JJA).

For the cold season (Figure 8), even though the Great Plains LLJ is the most inactive based on the description in section 3.2, it still has a clear diurnal variation. Compared with the results in summer, the diurnal cycle of Great Plains LLJ in winter is not that pronounced: It mainly occurs over the western Gulf of Mexico and southern Texas, with the frequency in the afternoon (18 UTC – 21 UTC) declining to 5-10%. The S-LLJ develops from 03 UTC, gradually generating two high-frequency (20%-25%) centers in mid- and southeastern Texas at 06 UTC – 12 UTC. As for the S-LLJ near Vancouver Island, it is hard to see the diurnal variability: There is only a slight magnitude growth of frequency from the afternoon (00 UTC) to the evening (06 UTC), and the coverage is almost the same.

删除了： significant

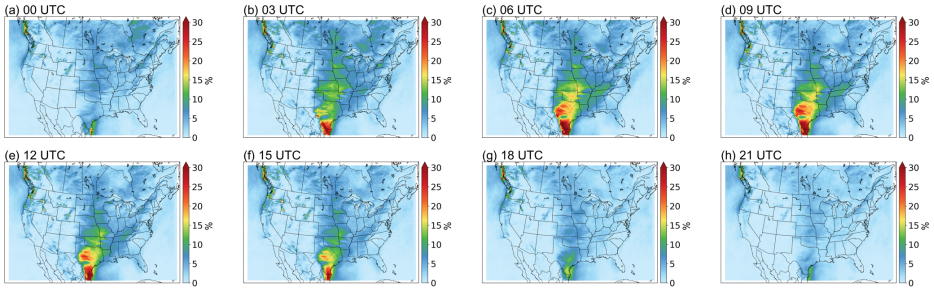

Figure 8. Diurnal frequency of S-LLJs in winter (DJF).

4 Formation and evolution mechanisms of various LLJs

Section 3's results illustrate the climatology of LLJs over North America, particularly their seasonal and diurnal features. To explain the mechanisms, the inertial oscillation theory from Blackadar (1957) is used. Using this theory, we start from the horizontal momentum equations and divide the actual horizontal wind u/v into two components—geostrophic wind u_g/v_g and ageostrophic wind u_a/v_a:

$$\frac{d(u_g + u_a)}{dt} = -\frac{1}{\rho}\frac{\partial P}{\partial x} + f\left(v_g + v_a\right) \tag{1.1}$$

$$\frac{d(v_g + v_a)}{dt} = -\frac{1}{\rho}\frac{\partial P}{\partial y} - f\left(u_g + u_a\right) \tag{1.2}$$

In which ρ is air density, P is pressure, and f is the Coriolis parameter. Assuming the horizontal pressure gradient is fixed, the geostrophic wind is a constant as well, which means $\frac{du_g}{dt} = \frac{dv_g}{dt} = 0$:

$$\frac{du_a}{dt} = -\frac{1}{\rho}\frac{\partial P}{\partial x} + f\left(v_g + v_a\right) \tag{2.2}$$

$$\frac{dv_a}{dt} = -\frac{1}{\rho}\frac{\partial P}{\partial y} - f\left(u_g + u_a\right) \tag{2.2}$$

When the definition of geostrophic wind $u_g = -\frac{1}{\rho f}\frac{\partial P}{\partial y}$ and $v_g = \frac{1}{\rho f}\frac{\partial P}{\partial x}$ is combined, the equation (2) is:

$$\frac{du_a}{dt} = fv_a \tag{3.1}$$

$$\frac{dv_a}{dt} = -fu_a \tag{3.2}$$

If $\frac{d}{dt}$ is taken to both sides of the equations (3), then we get $\frac{d^2u_a}{dt^2} = -f^2u_a$, and $\frac{d^2v_a}{dt^2} = -f^2v_a$, thereby:

$$u_a = c_1 cos(ft) + c_2 sin(ft) \quad (4.1)$$

$$v_a = c_2 cos(ft) - c_1 sin(ft) \quad (4.2)$$

Therefore, according to the equations (4), the ageostrophic wind should theoretically have a circle-pattern variation and the vector must rotate clockwise with a period of 2π/f (Blackadar, 1957; Van de Wiel et al., 2010). Under the condition of a constant geostrophic wind—when the ageostrophic vector rotates from the opposite to the same direction of geostrophic wind—the wind transitions from subgeostrophic to supergeostrophic. This change occurs because of decoupling with surface friction effects, then the wind gets unbalanced.

Other theories also help explain the formation of LLJs, such as the sloping-terrain thermodynamic mechanism (Holton, 1967) and background synoptic system forcing (Uccellini et al., 1987). To understand the characteristics of the LLJs in this study, three typical cases are analyzed: Great Plains S-LLJ, Quebec N-LLJ, and California coastal N-LLJ. The locations for extracting data are shown in Figure 1 (solid lines and stars a, b, c).

4.1 Great Plains S-LLJ

As Section 3's results show (see Fig. 7), the Great Plains S-LLJ typically occurs in summer and more frequently at night. To investigate its associated meteorological condition, this study extracts all the Great Plains S-LLJ cases occurs at the jet core in JJA. The jet core is defined by where the mean meridional wind is the strongest on the cross-section, and it locates at star A (shown in figure 1). The mean sea-level pressure and 800 hPa geopotential height are shown in Figure 9a and 9b, respectively. The background large-scale circulations indicate that, at all the time points when the Great Plains S-LLJ occurs, the range of the subtropical anticyclone extends east of the Great Plains at both ground and low-level atmosphere. A high-pressure ridge is located near the gulf coast of Mexico and Texas (Figure 9b). Thus, clearly, the zonal pressure/geopotential gradient in the central US guides the dominant southerly winds around this region. The cross-section in Figure 9c illustrates a strong baroclinicity and shows that the isentropic line incline moves from east to west, as is typical for the sloping-terrain heating effect (Holton, 1967). This effect generates an upslope wind on the east side of the slope, and the airstream gradually turns northward due to the Coriolis force, creating the southerly LLJs. On the other hand, as can be seen in the frequency cycle in Figure 9d, at noon local time (at the

删除了：，

selected point-a in Figure 1), the frequency of the Great Plains LLJ is very low (close to 0%), rising to more than 40% after 18 LST even if the radiation is not at the day's peak.

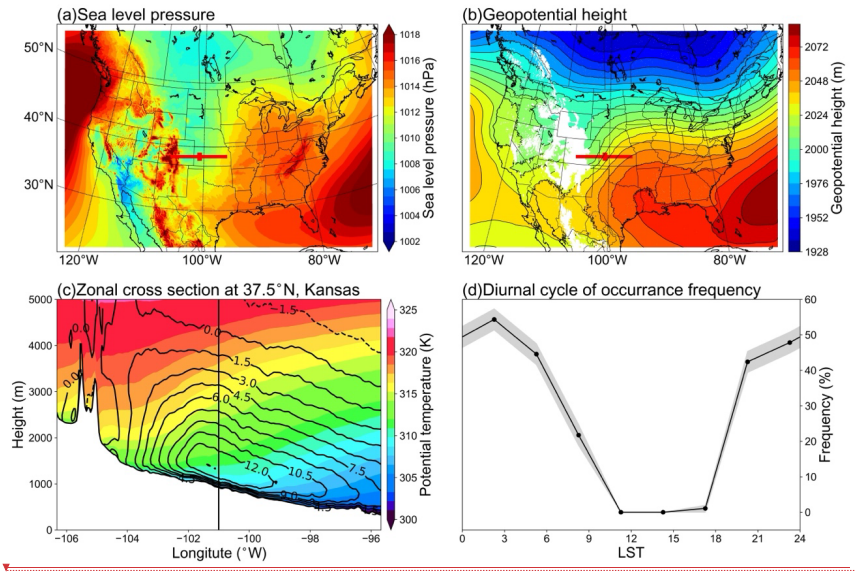

Figure 9. Background circulations of the Great Plains S-LLJ in JJA: (a) sea-level pressure, (b) geopotential height of 800 hPa, (c) cross section including meridional winds (lines) and potential temperature (shading), and (d) diurnal cycle of frequency, with the shaded 95% confidence intervals. The red lines and points in (a) and (b) show the position of cross-section and chosen jet core, the vertical line in (c) shows the zonal location of the chosen jet core.

To explain the nighttime enhancement of S-LLJ, we analyzed the wind vectors using inertial oscillation theory. To show more significant diurnal variation, all the time points, including the LLJs that did not occur, were considered. Figure 10a is the hodograph of jet-core winds at point-a near the Great Plains, and their temporal mean is computed at 3-hourly intervals in summer. It is noted here that the "jet-core" means the position where LLJ occurs the most frequently on the cross-section. Compared with the mean actual wind (blue arrow), the deviation at each local time shows a clear clockwise rotation. The wind speed begins increasing after 17 LST. Nevertheless, the analysis for Figure 9 indicates the sloping heating effect, meaning that the geostrophic wind is not fixed.

Thus, to obtain the ageostrophic winds, we computed the geostrophic components by pressure gradient and subtracted them from the actual airflow. According to the aforementioned definition of geostrophic wind, u_g and v_g are

删除了：

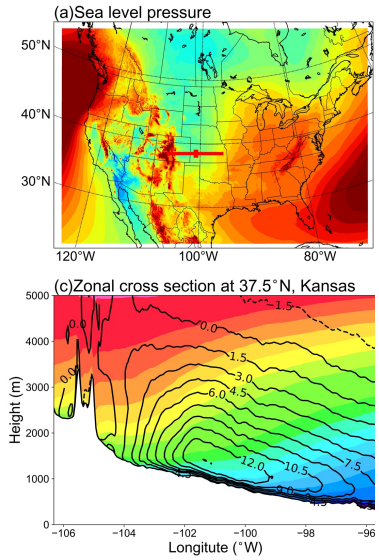

删除了：.

calculated by the horizontal pressure gradient $\frac{\partial P}{\partial y}$ and $\frac{\partial P}{\partial x}$, respectively. By choosing four grids surrounding point-a, we first interpolated the pressure value to the same level as the LLJ core height. Then, we adopted the central difference equation $\frac{\Delta P}{\Delta x} = \frac{P_{i+1}-P_{i-1}}{x_{i+1}-x_{i-1}}$ or $\frac{\Delta P}{\Delta y} = \frac{P_{i+1}-P_{i-1}}{y_{i+1}-y_{i-1}}$ to obtain the pressure gradients at point-a, where i is the index of the grid point at point-a.

Figures 10b and 10c display geostrophic wind vectors (blue arrows) and ageostrophic vectors (pink) at noon and midnight. The southerly geostrophic flows are much stronger in the afternoon (10b) than at midnight. The ageostrophic winds flow mostly in the opposite direction, limiting the actual wind speed. At night (10c), the geostrophic wind direction rotates clockwise from that of the afternoon as the pressure gradient changes. Considering the relative positions of blue and pink vectors at 23 LST and 01 LST, ageostrophic flow has rotated roughly 150 degrees to enhance the geostrophic winds, thereby creating a super-geostrophic state. Although the inertial oscillation theory can help explain some aspects of wind behavior, the real situation is more complex than initially thought. Figures 10b and 10c indicate that by 02 LST, the wind is almost entirely geostrophic with only negligible ageostrophic perturbations. This suggests that the diurnal changes in the geostrophic wind and pressure gradient may provide a complicating background that prevents the inertial oscillation theory from fully prevailing. While the inertial oscillation theory can provide valuable insights, it should not be relied upon as the sole explanation for LLJs at the Great Plains. Instead, a more comprehensive understanding of atmospheric dynamics is necessary to fully comprehend the behavior of the wind, particularly when dealing with diurnally changing conditions. Figure 10d compares different meridional wind components' amplitudes. The geostrophic wind contributes significantly to the southerly wind during the day, peaking at 14 LST (blue bars). The northerly ageostrophic wind (red bars) is highest during the day, indicating the strongest negative impact from friction. The meridional ageostrophic component decreases and eventually reverses at 23 LST, showing a process from sub- to super-geostrophic status. In summary, the thermodynamic circulation near the slopes of the Great Plains contributes to the strong southerly airflow, while the inertial oscillation plays a critical role in forming the nocturnal southerly LLJ.

删除了： .

删除了： green

删除了： green

删除了： green

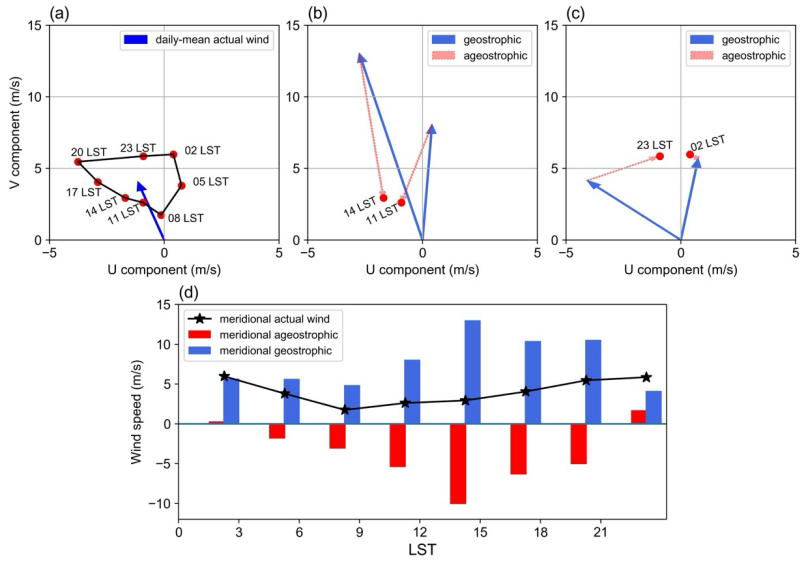

Figure 10. (a) Hodograph of jet-core winds for the Great Plains S-LLJ every 3 hours over the whole JJA (red dots – solid line) and the daily averaged actual wind velocity (blue vector); vectors of mean jet-core geostrophic winds (solid blue) and ageostrophic winds (dashed red) at (b) 11/14 LST and (c) 23/02 LST; (d) diurnal cycles of meridional components of actual (black line), geostrophic (blue bars), and ageostrophic winds (red bars).

4.2 Quebec N-LLJ

Similarly, for the Quebec N-LLJ that is typically observed in winter, we selected all the LLJ cases at point-b (see the position in Figure 1) in DJF to generate the background circulation pattern. The background large-scale circulations indicate that the northeastern coast of Canada lies to the west of a strong surface low-pressure system (Figure 11a), while in the lower troposphere, a ridge on the east side of Hudson Bay occupies the Labrador Plateau (Figure 11b). This combination brings the northerly momentum to the downstream eastern coast. In fact, the background circulation is consistent with the shallow baroclinic structure of Quebec N-LLJ in winter, that is, the thermal difference between relatively warm sea and cold land. The cross-section in Figure 11c shows the thermodynamic structure of this N-LLJ: A well-defined low-level jet core is located above land and close to the coastline (approximately 63°W). With a maximum wind speed of more than 16 m s-1 and a height of about 400 m, the jet core is located above the mixed layer under the warm air covering and on the land side. Notably, the steep isentropic lines slope towards the ocean and

删除了：

删除了： **green**

删除了： **blue**

删除了： **green**

finally sink at the position of 60°W. The onshore isentropic lines are flat and dense above the LLJ core, which means the environment is quite stable. This is helpful to maintain the structure of the LLJ, when vertical motion is inhibited, and horizontal wind is enhanced. Compared with the sloped isentropic lines in the Great Plain S-LLJ case (Figure 9c), the stability over Great Plain is not as high as in this case, so this difference in stability helps explain the variation in wind speeds between these two cases.

In addition, the diurnal cycle of frequency (Figure 11d) shows that the diurnal signal and peak frequency of Quebec N-LLJ are much weaker than the Great Plains S-LLJ, becoming weakest at noon and peaking at midnight, which is consistent with the results reported in Section 3. This diurnal variation can be explained by the baroclinicity near this region: At night in winter, the land temperature drops faster than the ocean temperature due to radiative cooling, enhancing the land-sea contrast and thereby the thermal wind above. The gentle slope on the east of the Labrador Plateau could generate the slope heating effect in the daytime. In this way, the related temperature gradient from east to west offsets the land-sea thermal difference.

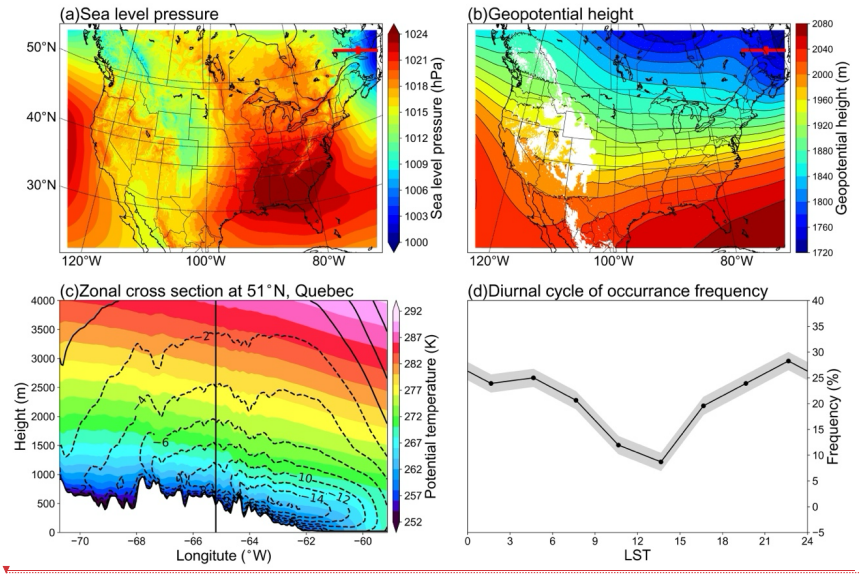

Figure 11. Background circulations of the Quebec N-LLJ in DJF: (a) sea-level pressure, (b) geopotential height of 800 hPa, (c) cross section including meridional winds (lines) and potential temperature (shading), and (d) diurnal cycle of frequency

删除了：

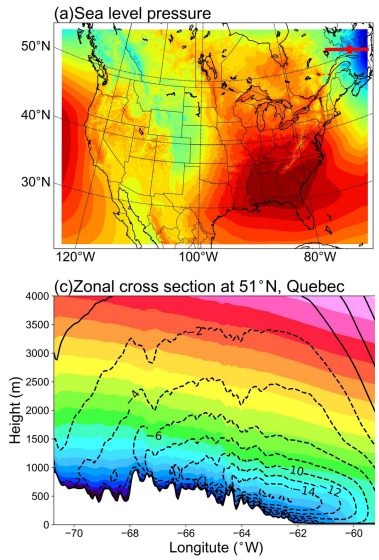

Figure 11. Same as Figure 9 but for Quebec N-LLJs in winter (DJF)….

with the shaded 95% confidence intervals. The red lines and points in (a) and (b) show the position of cross-section and chosen jet core, the vertical line in (c) shows the zonal location of the chose jet core.

As for the impact of inertial oscillation on the Quebec N-LLJ, the hodograph of averaged 3-hourly winds extracted at point-b (Figure 12a) also illustrates a clear clockwise rotation of wind deviations compared with the daily mean (blue arrow). Figure 12b and 12c show that the geostrophic and ageostrophic wind vectors contribute to the diurnal cycle in the afternoon and morning, respectively. Even though the direction of geostrophic wind changes significantly, the relative angles between ageostrophic and geostrophic arrows indicate that the ageostrophic flow rotates clockwise. The geostrophic wind is weakened by ageostrophic wind in the afternoon (Figure 12b), whereas the supergeostrophic state is generated in the morning (Figure 12c).

Focusing only on the meridional amplitudes validates this characteristic. In Figure 12d, the blue line that represents the mean actual meridional wind has the same diurnal trend as the frequency variation in Figure 11d. The northerly wind is weakest in the afternoon, peaking at night and in the early morning. Similarly, the variation of meridional geostrophic flow has a consistent phase with the actual meridional wind, which is explained by the baroclinic structure near the Quebec coast mentioned above. The meridional ageostrophic wind in this region also promotes the formation of N-LLJ. The ageostrophic wind drags the geostrophic component in the afternoon, before reversing to a consistent direction with the northerly geostrophic flow at night and in the morning. This trend is also the result of decreasing friction after sunset. Therefore, the evolution of Quebec N-LLJ derives from both inertial oscillation and land-sea thermal contrast in winter.

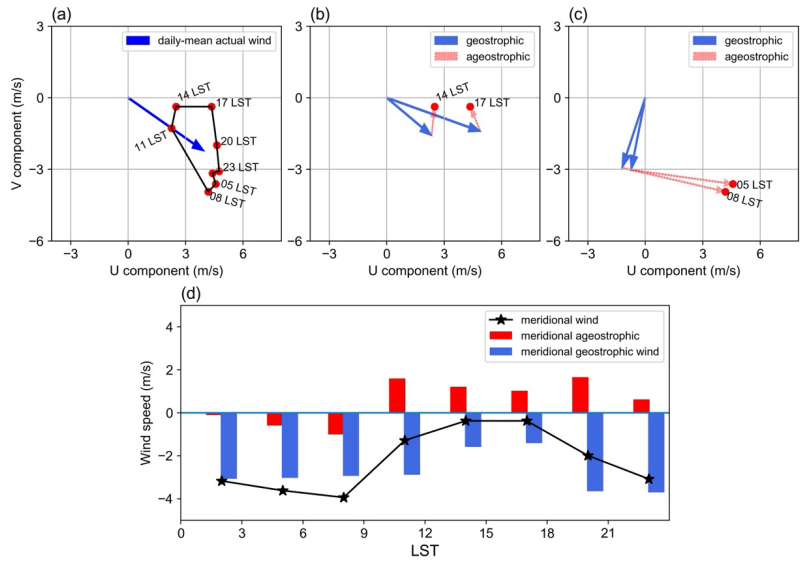

Figure 12. (a) Hodograph of jet-core winds for the Quebec N-LLJ every 3 hours over the whole DJF (red dots – solid line) and the daily averaged actual wind velocity (blue vector); vectors of mean jet-core geostrophic winds (solid blue) and ageostrophic winds (dashed red) at (b) 14/17 LST and (c) 05/08 LST; (d) diurnal cycles of meridional components of actual (black line), geostrophic (blue bars), and ageostrophic winds (red bars).

删除了：

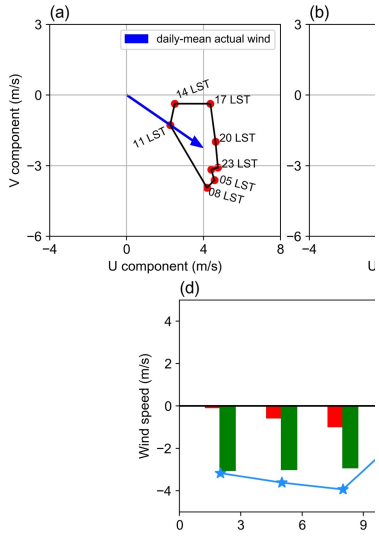

Figure 12. Same as Figure 10 but for Quebec N-LLJs in winter (DJF).

4.3 California coastal N-LLJ

The California coastal N-LLJ is similar to the one in Quebec, but it occurs more often in summer afternoons or evenings over the ocean. Figure 13a shows that a relatively strong high-pressure system is located on the east coast of the Pacific Ocean, trending NE-SW, although half of the structure is beyond the boundary of the domain. On the 800 hPa isobaric surface in Figure 13b, there is also an anticyclone system in the same location, whose eastern contour is roughly parallel to the coastline, guiding the airflow to the south. Therefore, this pair is also forced by the thermal difference between land and sea, but contrary to the LLJ in Quebec, in summer, when the California LLJ occurs frequently, it has the characteristics of the cool sea-hot land. Figure 13b also shows that the isobars near Cape Mendocino are relatively strong, making the ridge of high pressure extend northeastward of the Cape. This extension is generally believed to occur due to pressure perturbation caused when northerly winds converge at this position after being obstructed (Rahn and Parish, 2007). Regarding the cross-section structure shown in Figure 13c, the jet core is

located at steep isentropic lines above the ocean at a height of 500 m. On the coast of California, the LLJ is close to the mountains. The maximum central wind speed of California coastal LLJ exceeds 20 m s-1, whereas Quebec N-LLJ's max core wind is only about 14 m s-1. Based on baroclinicity, the isentropic lines slope towards the continent and finally sink near the coastline.

The core wind speed in California's coastal LLJ is higher than that of Quebec's LLJ because the land-sea contrast is more significant in summer than in winter and the formed sea breeze front generates flow convergence under the blockage caused by the west coast mountains. On the other hand, the atmosphere over the sea is more stable because the isentropic lines are flatter and denser than Quebec's case, which also favors the development of LLJ. In contrast, the east coast of Quebec is relatively gentle, which may account for its lower wind speed. California's LLJ occurs frequently at each time step, and its diurnal signal is weaker compared, for example, to the signal in the Great Plain S-LLJ. As well, the California signal stays at frequency of over 35%. California's LLJ occurs most frequently at around 18 LST and starts to decline after sunset, which is generally consistent with the coastal baroclinicity.

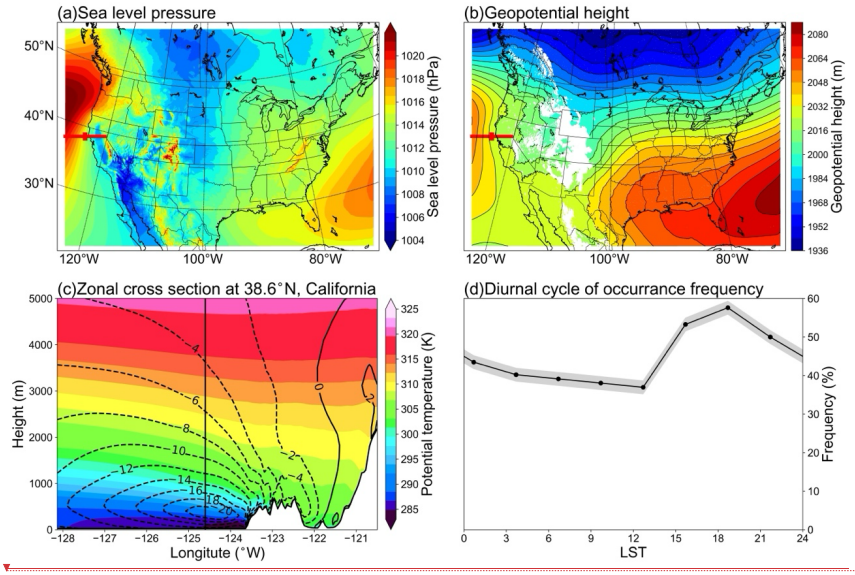

Figure 13. Background circulations of the California coastal N-LLJ in JJA: (a) sea-level pressure, (b) geopotential height of 800 hPa, (c) cross section including meridional winds (lines) and potential temperature (shading), and (d) diurnal cycle

删除了：Compared with the Quebec LLJ, California's

删除了：may be

删除了：Because California's

删除了：(13d), the

删除了：weak

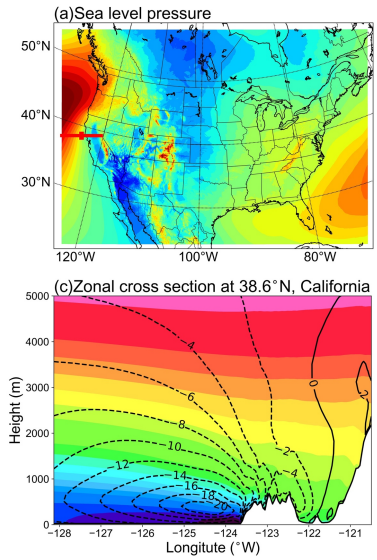

删除了：

Figure 13. Same as Figure 9 but for California Coastal S-LLJ in summer (JJA).

of frequency with the shaded 95% confidence intervals. The red lines and points in (a) and (b) show the position of cross-section and chosen jet core, the vertical line in (c) shows the zonal location of the chosen jet core.

The wind deviations for California's N-LLJ shown in the hodograph (Figure 14a) still have a clockwise rotation in 24 hours. However, compared with the magnitude of the daily mean jet-core wind, this diurnal cycle is not quite as obvious as the cycle for Quebec and Great Plain LLJs, but it is similar to the frequency cycle shown in Figure 13d. In comparison between geostrophic and ageostrophic winds (Figure.14b and 14c), during the afternoon (15 and 18 LST), the amplitude of geostrophic wind is the largest, and the ageostrophic flow diminishes the geostrophic wind. However, in the morning 12 hours later, the relative angle between ageotrophic and geostrophic vectors does not change, meaning that the ageostrophic wind is still weakening the geostrophic wind and that there is no rotation of the ageostrophic wind, as Blackadar inertial oscillation theory describes. Figure 14d helps to explain the change in meridional winds. Looking at the magnitudes of ageostrophic winds, one can see that all are weak and southerly and that they do not exhibit a significant diurnal signal. Furthermore, the change of geostrophic wind is highly consistent with the trend of the actual meridional wind. Thus, the N-LLJ in California can be considered mostly as geostrophic and the diurnal variation as being related to the change in geostrophic winds.

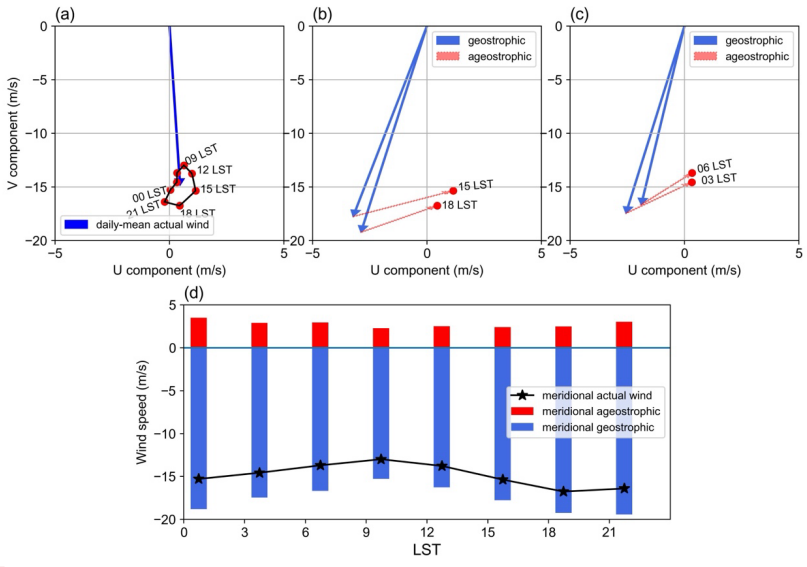

删除了：

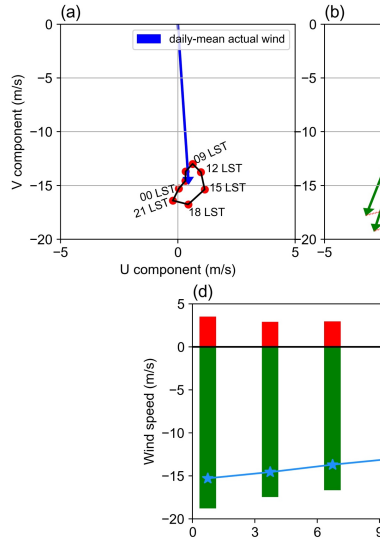

Figure 14. Same as Figure 10 but for California Coastal S-LLJ in summer (JJA).

Figure 14. (a) Hodograph of jet-core winds for the California coastal N-LLJ every 3 hours over the whole JJA (red dots – solid line) and the daily averaged actual wind velocity (blue vector); vectors of mean jet-core geostrophic winds (solid blue) and ageostrophic winds (dashed red) at (b) 15/18 LST and (c) 03/06 LST; (d) diurnal cycles of meridional components of actual (black line), geostrophic (blue bars), and ageostrophic winds (red bars).

5 Discussion and conclusion

This study applied a convection-permitting WRF model to generate the climatology of LLJs in North America. The previous research for LLJs mainly focused on observation data, which have no fine coverage in temporal or spatial resolution. The studies using in-situ observations may ignore some important features. Despite their better coverage, reanalysis datasets usually have a coarse spatial resolution, especially in the vertical direction, and can introduce large inaccuracies in the identification of LLJs. In addition, the application of general numerical modeling cannot avoid the uncertainty caused by parameterizing small-scale physical processes. In contrast, high-resolution convection-permitting climate simulations can provide relatively more comprehensive descriptions of LLJs, especially for areas with complex geographic conditions or regions that lack soundings. Previous studies using high-resolution models conducted case analyses only of LLJs in a specific region (Aird et al., 2022). By expanding the target domain to the whole of North America and revealing the climatological characteristics of LLJs in different regions and scales, this paper provides an accurate reference for future research on LLJ-related processes in North America.

删除了： reliable and accurate

The convection-permitting WRF model is able to recapture some LLJs that have been previously studied, such as the Great Plain S-LLJ and the California coastal N-LLJ in the eastern Pacific Ocean and has obtained relatively consistent results. The results indicate that the S-LLJ in the central US Plain is the most frequent and active in warm seasons and that three critical high-frequency centers occur in summer: the northeast Mexico-Texas border, west-central Texas, and western Oklahoma to southern Kansas. This last result is consistent with the climatology generated by Doubler et al. (2015) using the NARR reanalysis data, but the patterns here are more representative of the topographic features in central and southern Texas. In addition, compared with the 40-year rawinsonde climatology in the central US by Walters et al. (2008), our study reveals that the S-LLJ frequency range of these three centers in the central US in summer is 25%-30%, which is slightly lower than the 35% reported in the 2008 study. However, given the underestimated frequencies of 15%-20% in NARR climatology, there is an advantage of using high-resolution simulations in the vertical direction.

The convection-permitting simulation can also capture LLJs that were poorly detected previously using coarser resolution models and observational datasets. The winter N-LLJs over the eastern Rocky Mountains described in this paper are generally distributed over the central US from the Dakotas to Oklahoma with a low frequency (>10%) and over several sporadic small areas with a high frequency (>20%) along the boundary of the Rockies. The main seasonal/diurnal variations identified in this study agree with those seen using rawinsonde data (Walters et al., 2008) and NARR reanalysis (Douber et al., 2015). But the frequency of the LLJ occurrence over Nebraska-Kansas was underestimated in both convection-permitting simulations (~10%) and NARR (~7%), while high-frequency hot spots from Alberta to Colorado were not detected in either of the above-mentioned studies, probably because measurements are lacking in these regions. The high-resolution simulation also detected LLJs on which researchers have hardly focused: N-LLJs near the eastern Quebec coast and in the Appalachians Mountains, as well as an S-LLJ over the British Columbia coast. In the work of Douber et al. (2015), these LLJs were shown in the climatology patterns, but the 4-km WRF simulation offered more detailed descriptions of their locations. For example, this study found that the Appalachian N-LLJ extends from Georgia to the northwestern Atlantic, especially on summer nights (03 UTC – 06 UTC), while NARR only captured LLJ occurrences over the middle coast of the Atlantic. The maximum frequency (7-10%) detected in the NARR study is also less than what is illustrated here. As for the Quebec N-LLJ, the 4-km WRF revealed that it mostly occurs onshore near the coast with a frequency of over 25% in winter, but NARR only provided a coarse occurrence distribution over northeastern Canada.

To investigate the significance of LLJs in different regions, Figures 15 and 16 demonstrate the impact of the Great Plains S-LLJ and Quebec N-LLJ, respectively, on downstream extreme precipitation during their active seasons. Figure 15a illustrates the 90th percentile of summer precipitation in the central United States, indicating that 90% of the precipitation in most areas falls within the range of 1.0-2.0 mm/hour. However, Figure 15b shows the ratio of strong events related to LLJs (counted if the precipitation is > 90th percentile when a LLJ occurs) to all strong events, with the red outline on the map indicating the approximate location of the low-level jet stream. It is evident that in the lower reaches of the S-LLJ in the Great Plain, particularly in the north-central United States, nearly 50% of the heavy precipitation events are associated with the flourishing low-level jet stream. Furthermore, Figure 15c displays the average precipitation of all LLJ-related strong events. Compared with Figure 15a, some areas of Nebraska and Minnesota experience rainfall of up to 6mm/hour. These findings highlight the significant role played by LLJ in

删除了： Convection
删除了： simulations
删除了： the
删除了： barely

modulating summer precipitation. Similarly, for the Quebec N-LLJ in winter (Fig. 16), it contributes more than 25% of the strong events of precipitation in the Gulf of St. Lawrence during winter (Fig. 16b). Figure 16c further reveals that, in comparison to the 90th percentile rainfall, the extreme precipitation from Quebec to Maine is approximately 1mm/hr higher. Particularly during the cold season when a substantial portion of precipitation is snow, the N-LLJs can also be seen as the factors of snowstorms in this region. In summary, research on the importance of LLJs includes not only the field of extreme precipitation, but also local wind energy production, air pollution dispersion, wildfires, etc. (Jain & Flannigan 2021, Lin et al. 2022, Weide Luiz & Fiedler 2022). There is no doubt that the high-resolution regional climate model presented in this paper provides ample coverage and details about LLJs in North America, to support analysis in these fields, particularly at the national level. With a grid spacing as small as 4 km, researchers can even employ the wind profiles from model output to investigate small-scale areas, such as wind farms or wildfire ignition sites.

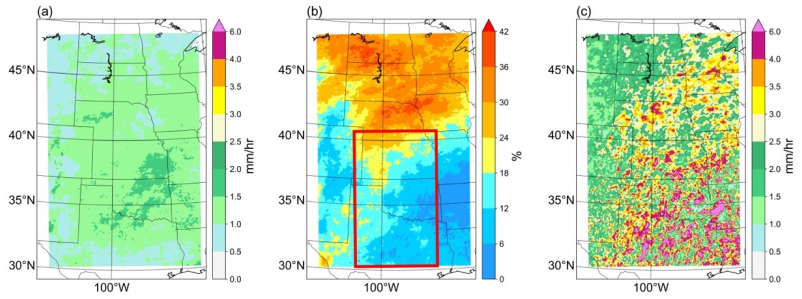

Figure 15. (a) 90th percentile of summer precipitation rate over Central US; (b) The ratio of LLJ-related strong rainfall events to all strong events, the red outline represents the location of Great Plain S-LLJ; (c) Averaged precipitation rate of LLJ-related strong events.

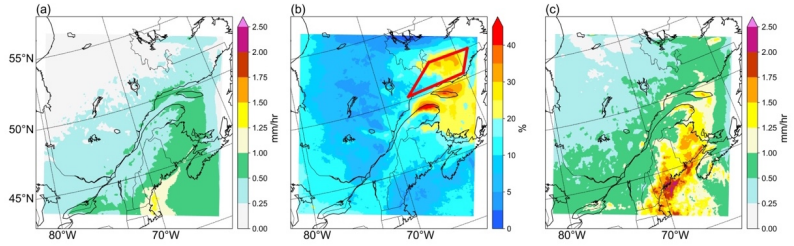

Figure 16. (a) 90th percentile of winter precipitation rate over Southeastern Canada; (b) The ratio of LLJ-related strong rainfall events to all strong events, the red outline represents the location of Quebec N-LLJ; (c) Averaged precipitation rate of LLJ-related strong events.

Based on the inertial oscillation theory (Blackadar, 1957) and the baroclinic theory near complex terrain (Holton, 1967), this paper also analyzed the background and formation mechanisms of three LLJs: the Great Plain S-LLJ, Quebec N-LLJ, and California coastal N-LLJ. Generally, all these LLJs are impacted by the thermodynamic circulations generated near their topography. The Great Plain S-LLJ is affected by slope heating, and the LLJs over Quebec and California are associated with the sea-land contrast. When the geostrophic and ageostrophic components of the LLJs are compared, results show that the inertial oscillation better explains the night enhancement of the Great Plains S-LLJ and that the diurnal feature of the Quebec N-LLJ is influenced by the combination of the Holton and Blackadar theories. As for the California coastal N-LLJ, no supergeostrophic state is found, making coastal baroclinicity variation a dominant factor for this LLJ's evolution the geostrophic wind changes.

The LLJs climatology introduced in this research adds to the existing knowledge of characteristics of the low-level wind maxima in North America, thus helping researchers obtain more reliable references about LLJs in this domain. Meanwhile, with the high-resolution features, it can provide more robust explanations for other interdisciplinary fields. The research also advances knowledge about the formation of three dominant LLJs. Although the 13-year simulation is likely too short to provide an ideal long-term climatic analysis, it is a less expensive option for finer numerical modeling in large domains. But it is also believed that with the advancement of technology, there will be longer high-resolution simulations in the future. Future work will address the features and formation mechanisms of the small-scale low-level wind maxima that have yet to be investigated.

Acknowledgments

All authors thank the support of the Global Water Futures Program by the Canada First Research Excellence and the NSERC Discovery Grant.

Data Availability Statement

The WRF simulation over CONUS can be accessed at Research Data Archive of NCAR https://rda.ucar.edu/datasets/ds612.0/.

Author contribution

Xiao Ma: Conceptualization; data curation; formal analysis; investigation; methodology; visualization; writing-original draft.

Yanping Li: Conceptualization; funding acquisition; investigation; methodology; project administration; supervision; validation; writing-review and editing.

Zhenhua Li: Data curation; methodology; validation; visualization; writing-review and editing.

Fei Huo: Data curation; methodology; validation; visualization; writing-review and editing.

Competing interests

All authors disclosed no relevant relationships.

Appendix

Winter LLJs captured by ERA5 Dataset

The convection-permitting WRF simulation exhibited excellent performance in investigating well-known LLJ systems, such as the California coastal N-LLJ and the Great Plains S-LLJ. Moreover, this appendix validates WRF-simulated significant winter jet systems over North America using the ERA5 reanalysis dataset. ERA5 is a global atmospheric reanalysis dataset produced by the European Centre for Medium-Range Weather Forecasts (ECMWF). It provides hourly data on a horizontal grid space of approximately 31 km, and the time range covers from 1979 till the present. ERA5 data is widely used in climate research, weather forecasting, and various applications that require high-quality atmospheric data.

The validation period is the same as the WRF simulation (2000-2013). From the Figure A1 below, it is evident that during winter, a greater number of significant N-LLJ systems in the North American continent are mostly concentrated in eastern Canada. In most parts of Newfoundland and southeastern Quebec, the occurrence frequency of N-LLJs exceeds 15%, and the maximum can even surpass 25%. However, in the WRF simulation (Figure 3d), the model can only capture N-LLJs on the north bank of the St. Lawrence River due to the northern boundary of the study domain overlapping with the Quebec border. In comparison, the WRF-simulated frequency of N-LLJs in southeastern Quebec essentially exceeds 25%, overestimated by about 5% compared to the ERA5 reanalysis. Additionally, it is worth noting that the N-LLJs along the downstream of Rockies are also identified in the ERA5 dataset. The areas where the frequency exceeds 5% are mainly distributed from Alberta to northern Texas, consistent with the findings in Section 3.2.1. Moreover, the high-value center (>10%) is located in central Kansas. In terms of the differences between the two datasets, the results of the WRF simulation match more geographical features and reveal scattered high-value spots (>15%) in some regions with special terrains (see Figure 3d). Furthermore, the winter Great Plains S-LLJs in ERA5 reanalysis exhibit similar features, with frequencies ranging from around 15% to 20% in southern Texas. In summary, the WRF model can accurately capture the features of winter LLJ systems, which are validated by the ERA5 reanalysis dataset over northern America. Even though the frequency of LLJs occurrence is overestimated, the convection-permitting WRF simulation can provide detailed descriptions of LLJs near complex terrains.

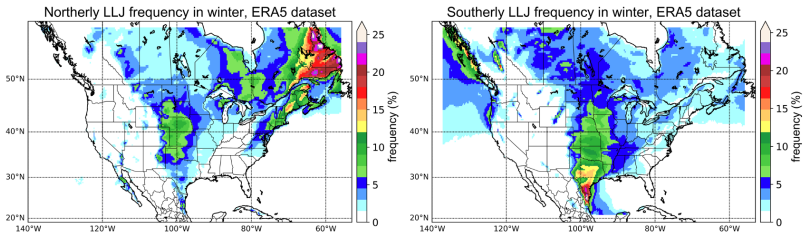

Figure A1. Winter occurrence frequency of N-LLJs (left) and S-LLJs (right).

Data Availability Statement

The ERA5 dataset is available on the Copernicus Climate Change Service Information website.

https://cds.climate.copernicus.eu/#!/home

References

Aird, J. A., Barthelmie, R. J., Shepherd, T. J. and Pryor, S. C.: Occurrence of Low-Level Jets over the Eastern U.S. Coastal Zone at Heights Relevant to Wind Energy, Energies, 15(2), 445, doi:10.3390/en15020445, 2022.

Blackadar, A. K.: Boundary Layer Wind Maxima and Their Significance for the Growth of Nocturnal Inversions, Bulletin of the American Meteorological Society, 38(5), 283–290, doi:10.1175/1520-0477-38.5.283, 1957.

Bonner, W. D.: CLIMATOLOGY OF THE LOW LEVEL JET, Monthly Weather Review, 96(12), 833–850, doi:10.1175/1520-0493(1968)096<0833:cotllj>2.0.co;2, 1968.

Chen, G. T.-J., Wang, C.-C. and Lin, D. T.-W.: Characteristics of Low-Level Jets over Northern Taiwan in Mei-Yu Season and Their Relationship to Heavy Rain Events, Monthly Weather Review, 133(1), 20–43, doi:10.1175/mwr-2813.1, 2005.

Doubler, D. L., Winkler, J. A., Bian, X., Walters, C. K. and Zhong, S.: An NARR-Derived Climatology of Southerly and Northerly Low-Level Jets over North America and Coastal Environs, Journal of Applied Meteorology and Climatology, 54(7), 1596–1619, doi:10.1175/jamc-d-14-0311.1, 2015.

Du, Y. and Chen, G.: Heavy Rainfall Associated with Double Low-Level Jets over Southern China. Part II: Convection Initiation, Monthly Weather Review, 147(2), 543–565, doi:10.1175/mwr-d-18-0102.1, 2019.

Frisch, A. S., Orr, B. W. and Martner, B. E.: Doppler Radar Observations of the Development of a Boundary-Layer Nocturnal Jet, Monthly Weather Review, 120(1), 3–16, doi:10.1175/1520-0493(1992)120<0003:drootd>2.0.co;2, 1992.

Fu, P., Zhu, K., Zhao, K., Zhou, B. and Xue, M.: Role of the nocturnal low-level jet in the formation of the morning precipitation peak over the Dabie Mountains, Advances in Atmospheric Sciences, 36(1), 15–28, doi:10.1007/s00376-018-8095-5, 2018.

Gadde, S. N. and Stevens, R. J. A. M.: Effect of low-level jet height on wind farm performance, Journal of Renewable and Sustainable Energy, 13(1), 013305, doi:10.1063/5.0026232, 2021.

692 Hodges, D. and Pu, Z.: Characteristics and Variations of Low-Level Jets and Environmental Factors Associated with
693 Summer Precipitation Extremes over the Great Plains, Journal of Climate, 32(16), 5123–5144, doi:10.1175/jcli-d-18-
694 0553.1, 2019.

695 Hoffmann, L. and Spang, R.: An assessment of tropopause characteristics of the ERA5 and era-interim meteorological
696 reanalyses, Atmospheric Chemistry and Physics, 22(6), 4019–4046, doi:10.5194/acp-22-4019-2022, 2022.

697 Holton, J. R.: The diurnal boundary layer wind oscillation above sloping terrain, Tellus, 19(2), 199–205,
698 doi:10.1111/j.2153-3490.1967.tb01473.x, 1967.

699 Hong, S.-Y., Noh, Y. and Dudhia, J.: A New Vertical Diffusion Package with an Explicit Treatment of Entrainment
700 Processes, Monthly Weather Review, 134(9), 2318–2341, doi:10.1175/mwr3199.1, 2006.

701 Hu, X.-M., Klein, P. M., Xue, M., Lundquist, J. K., Zhang, F. and Qi, Y.: Impact of Low-Level Jets on the Nocturnal
702 Urban Heat Island Intensity in Oklahoma City, Journal of Applied Meteorology and Climatology, 52(8), 1779–1802,
703 doi:10.1175/jamc-d-12-0256.1, 2013.

704 Iacono, M. J., Delamere, J. S., Mlawer, E. J., Shephard, M. W., Clough, S. A. and Collins, W. D.: Radiative forcing
705 by long-lived greenhouse gases: Calculations with the AER radiative transfer models, Journal of Geophysical
706 Research, 113(D13), doi:10.1029/2008jd009944, 2008.

707 Jain, P. and Flannigan, M.: The relationship between the Polar Jet Stream and extreme wildfire events in North
708 America, Journal of Climate, 1–59, doi:10.1175/jcli-d-20-0863.1, 2021.

709 Jiménez-Sánchez, G., Markowski, P. M., Jewtoukoff, V., Young, G. S. and Stensrud, D. J.: The Orinoco Low-Level
710 Jet: An Investigation of Its Characteristics and Evolution Using the WRF Model, Journal of Geophysical Research:
711 Atmospheres, 124(20), 10696–10711, doi:10.1029/2019jd030934, 2019.

712 Kurkute, S., Li, Z., Li, Y. and Huo, F.: Assessment and projection of the water budget over Western Canada using
713 convection-permitting weather research and forecasting simulations, Hydrology and Earth System Sciences, 24(7),
714 3677–3697, doi:10.5194/hess-24-3677-2020, 2020.

Li, Y., Li, Z., Zhang, Z., Chen, L., Kurkute, S., Scaff, L. and Pan, X.: High-resolution regional climate modeling and projection over Western Canada using a weather research forecasting model with a pseudo-global warming approach, Hydrology and Earth System Sciences, 23(11), 4635–4659, doi:10.5194/hess-23-4635-2019, 2019.

Lin, Y., Wang, C., Yan, J., Li, J. and He, S.: Observation and simulation of low-level jet impacts on 3D urban heat islands in Beijing: A case study, Journal of the Atmospheric Sciences, 79(8), 2059–2073, doi:10.1175/jas-d-21-0245.1, 2022.

Liu, C., Ikeda, K., Rasmussen, R., Barlage, M., Newman, A. J., Prein, A. F., Chen, F., Chen, L., Clark, M., Dai, A., Dudhia, J., Eidhammer, T., Gochis, D., Gutmann, E., Kurkute, S., Li, Y., Thompson, G. and Yates, D.: Continental-scale convection-permitting modeling of the current and future climate of North America, Climate Dynamics, 49(1–2), 71–95, doi:10.1007/s00382-016-3327-9, 2016.

Ma, X., Li, Y. and Li, Z.: The projection of Canadian wind energy potential in future scenarios using a convection-permitting regional climate model, Energy Reports, 8, 7176–7187, doi:10.1016/j.egyr.2022.05.122, 2022.

Miao, Y., Guo, J., Liu, S., Wei, W., Zhang, G., Lin, Y., Zhai, P., Zhai, P., Lin, Y., Zhang, G., Wei, W., Liu, S., Guo, J. and Miao, Y.: The Climatology of Low-Level Jet in Beijing and Guangzhou, China, Journal of Geophysical Research: Atmosphere, 123(5), 2816–2830, doi:10.1002/2017jd027321, 2018.

Mitchell, M. J., Arritt, R. W. and Labas, K.: A Climatology of the Warm Season Great Plains Low-Level Jet Using Wind Profiler Observations, Weather and Forecasting, 10(3), 576–591, doi:10.1175/1520-0434(1995)010<0576:acotws>2.0.co;2, 1995.

Montini, T. L., Jones, C. and Carvalho, L. M. V.: The South American Low-Level Jet: A New Climatology, Variability, and Changes, Journal of Geophysical Research: Atmospheres, 124(3), 1200–1218, doi:10.1029/2018jd029634, 2019.

Munday, C., Washington, R. and Hart, N.: African Low-Level Jets and Their Importance for Water Vapor Transport and Rainfall, Geophysical Research Letters, 48(1), doi:10.1029/2020gl090999, 2021.

737 Niu, G.-Y., Yang, Z.-L., Mitchell, K. E., Chen, F., Ek, M. B., Barlage, M., Kumar, A., Manning, K., Niyogi, D.,
738 Rosero, E., Tewari, M. and Xia, Y.: The community Noah land surface model with multiparameterization options
739 (Noah-MP): 1. Model description and evaluation with local-scale measurements, Journal of Geophysical Research,
740 116(D12), doi:10.1029/2010jd015139, 2011.

741 Parish, T. R.: Forcing of the Summertime Low-Level Jet along the California Coast, Journal of Applied Meteorology,
742 39(12), 2421–2433, doi:10.1175/1520-0450(2000)039<2421:fotsll>2.0.co;2, 2000.

743 Rahn, D. A. and Parish, T. R.: Diagnosis of the Forcing and Structure of the Coastal Jet near Cape Mendocino Using
744 In Situ Observations and Numerical Simulations, Journal of Applied Meteorology and Climatology, 46(9), 1455–1468,
745 doi:10.1175/jam2546.1, 2007.

746 Rife, D. L., Pinto, J. O., Monaghan, A. J., Davis, C. A. and Hannan, J. R.: Global Distribution and Characteristics of
747 Diurnally Varying Low-Level Jets, Journal of Climate, 23(19), 5041–5064, doi:10.1175/2010jcli3514.1, 2010.

748 Saulo, C., Ruiz, J. and Skabar, Y. G.: Synergism between the Low-Level Jet and Organized Convection at Its Exit
749 Region, Monthly Weather Review, 135(4), 1310–1326, doi:10.1175/mwr3317.1, 2007.

750 Shapiro, A., Fedorovich, E. and Rahimi, S.: A unified theory for the Great Plains Nocturnal low-level jet, Journal of
751 the Atmospheric Sciences, 73(8), 3037–3057, doi:10.1175/jas-d-15-0307.1, 2016.

752 Smith, E. N., Gebauer, J. G., Klein, P. M., Fedorovich, E. and Gibbs, J. A.: The Great Plains Low-Level Jet during
753 PECAN: Observed and Simulated Characteristics, Monthly Weather Review, 147(6), 1845–1869, doi:10.1175/mwr-
754 d-18-0293.1, 2019.

755 Soares, P. M., Lima, D. C., Semedo, A., Cardoso, R. M., Cabos, W. and Sein, D. V.: Assessing the climate change
756 impact on the North African offshore surface wind and coastal low-level jet using coupled and uncoupled regional
757 climate simulations, Climate Dynamics, 52(11), 7111–7132, doi:10.1007/s00382-018-4565-9, 2018.

758 Stensrud, D. J.: Importance of Low-Level Jets to Climate: A Review, Journal of Climate, 9(8), 1698–1711,
759 doi:10.1175/1520-0442(1996)009<1698:iolljt>2.0.co;2, 1996.

760 Sullivan, J. T., Rabenhorst, S. D., Dreessen, J., McGee, T. J., Delgado, R., Twigg, L. and Sumnicht, G.: Lidar
761 observations revealing transport of O3 in the presence of a nocturnal low-level jet: Regional implications for “next-
762 day” pollution, Atmospheric Environment, 158, 160–171, doi:10.1016/j.atmosenv.2017.03.039, 2017.

763 Tang, Y., Winkler, J., Zhong, S., Bian, X., Doubler, D., Yu, L. and Walters, C.: Future changes in the climatology of
764 the Great Plains low-level jet derived from fine resolution multi-model simulations, Scientific Reports, 7(1),
765 doi:10.1038/s41598-017-05135-0, 2017.

766 Uccellini, L. W., Petersen, R. A., Kocin, P. J., Brill, K. F. and Tuccillo, J. J.: Synergistic Interactions between an
767 Upper-Level Jet Streak and Diabatic Processes that Influence the Development of a Low-Level Jet and a Secondary
768 Coastal Cyclone, Monthly Weather Review, 115(10), 2227–2261, doi:10.1175/1520-
769 0493(1987)115<2227:sibaul>2.0.co;2, 1987.

770 Van de Wiel, B. J., Moene, A. F., Steeneveld, G. J., Baas, P., Bosveld, F. C. and Holtslag, A. A.: A conceptual view
771 on inertial oscillations and nocturnal low-level jets, Journal of the Atmospheric Sciences, 67(8), 2679–2689,
772 doi:10.1175/2010jas3289.1, 2010.

773 Walters, C. K. and Winkler, J. A.: Airflow Configurations of Warm Season Southerly Low-Level Wind Maxima in
774 the Great Plains. Part I: Spatial and Temporal Characteristics and Relationship to Convection, Weather and
775 Forecasting, 16(5), 513–530, doi:10.1175/1520-0434(2001)016<0513:acowss>2.0.co;2, 2001.

776 Walters, C. K., Winkler, J. A., Shadbolt, R. P., van Ravensway, J. and Bierly, G. D.: A Long-Term Climatology of
777 Southerly and Northerly Low-Level Jets for the Central United States, Annals of the Association of American
778 Geographers, 98(3), 521–552, doi:10.1080/00045600802046387, 2008.

779 Weide Luiz, E. and Fiedler, S.: Spatiotemporal observations of nocturnal low-level jets and impacts on wind
780 power production, Wind Energy Science, 7(4), 1575–1591, doi:10.5194/wes-7-1575-2022, 2022.

781 Zhang, Y., Xue, M., Zhu, K. and Zhou, B.: What is the main cause of diurnal variation and nocturnal peak of summer
782 precipitation in Sichuan Basin, China? the key role of boundary layer low-level jet inertial oscillations, Journal of
783 Geophysical Research: Atmospheres, 124(5), 2643–2664, doi:10.1029/2018jd029834, 2019.

784 Zhong, S., Fast, J. D. and Bian, X.: A Case Study of the Great Plains Low-Level Jet Using Wind Profiler Network
785 Data and a High-Resolution Mesoscale Model, Monthly Weather Review, 124(5), 785–806, doi:10.1175/1520-
786 0493(1996)124<0785:acsotg>2.0.co;2, 1996.